10

Orographic drag parameterizations

10.1 Introduction

Mountains are one of the most visually stunning features of the landscape. Created by the collision of tectonic plates and the eruption of volcanoes, and then sculpted by rain and winds, mountains are a source of both inspiration and wonder. The Greek gods were believed to dwell on top of Mount Olympus, while folklore suggests that wise men and women seek mountain tops to find solitude and ponder the fate of the universe. Yet in reality, mountains are obstacles to most forms of transportation and acted as nearly impenetrable barriers to many early human communities. In a similar manner, mountains also influence the atmosphere by acting as obstacles to air flow and their effects are included in parameterization schemes for many numerical weather prediction and climate simulation models.

The flow of water in a fast-moving mountain stream provides a useful analogy to the influences of mountains on the atmosphere. The surface of the water in such a stream is often far from uniform, and clearly shows the influence of submerged obstacles, such as large rocks, that act to perturb the water surface both slightly ahead of and downstream from the obstacles. Mountains act in a similar fashion to perturb the atmospheric flow. This occurs because a stable atmospheric stratification creates buoyancy forces that act to return vertically displaced parcels to their equilibrium levels and because slight ascent often leads to saturation of the atmosphere and cloud formation (Smith 1979).

Analyses from the output of medium-range numerical weather prediction models and general circulation models in the 1970s and 1980s during the northern hemisphere cold season indicate that the zonally averaged upper-tropospheric flow was too strong in the midlatitudes after several days of prediction time (Lilly 1972; Palmer *et al.* 1986; Kim *et al.* 2003). This systematic error influenced the predicted values of sea-level pressure, low-level winds,

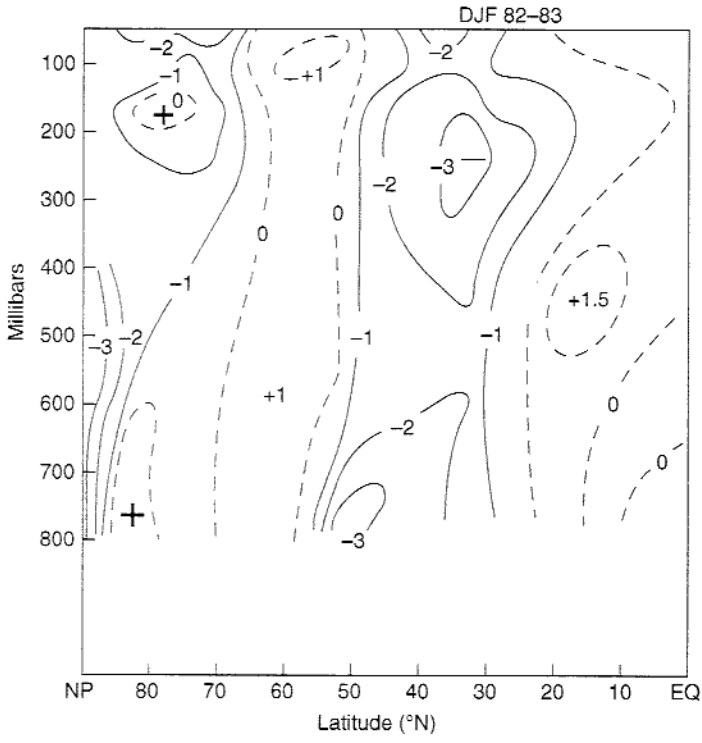

Figure 10.1. Residual term ($m\,s^{-1}\,d^{-1}$) from the zonal mean momentum budget calculated using uninitialized global analyses from December 1982 to February 1983 and attributable to subgrid-scale motions. Note the vertical coherence in the drag between 30° and 50° N and the occurrence of both low-level and upper-level minima. From Palmer *et al.* (1986).

geopotential heights, and the evolution of extratropical cyclones (Palmer *et al.* 1986). Since the model-produced zonally averaged wind speeds agreed in many other respects with observations, this overprediction of the midlatitude westerly subtropical jet suggested that an important physical process was not included (Lilly 1972). Zonal mean momentum budget calculations from uninitialized forecast model analyses also indicated that the residual terms, representing the effects of subgrid-scale motions, produce a drag in midlatitudes during the cool season (Fig. 10.1) further strengthening the argument that some subgrid-scale process was not incorporated in the models (Palmer *et al.* 1986).

Further studies indicate that this cold season wind speed error is due to the lack of sufficient drag from rugged mountain ranges. At low levels, mountains can produce flow blocking under stable atmospheric stratifications, changing the effective mountain height and influencing the stationary waves in the atmosphere (Wallace *et al.* 1983). However, as described by Palmer *et al.*

(1986), in stratified flow a drag force can be imposed on the atmosphere via internal gravity waves. These waves have horizontal wavelengths of ~6 km for flow over a hill of width 1 km and propagate vertically into the atmosphere. Wave breaking occurs when the waves reach a critical level; therefore, these internal gravity waves are able to create an upper-level drag on the atmospheric flow (Lindzen 1981). If the model grid spacing is greater than 5–10 km, then there can be a significant underestimation of the drag force exerted by rugged mountain ranges since these waves and the terrain features that generate them are not resolved adequately by the model (Clark and Miller 1991). This systematic model wind speed error is much smaller or negligible during the warm season, when the atmospheric stratification and surface winds are weaker. It also is negligible when the elevated terrain varies smoothly, such as over plateaus, where there is little subgrid variation in terrain height.

10.2 Simple theory

The response of the atmosphere to changes in terrain, such as mountain ranges and more isolated hills, is complicated because it depends upon the ever evolving atmospheric stratification. One measure of atmospheric stability is the Brunt-Väisälä frequency N (s^{-1}), where

$$N^2 = \frac{g}{\theta}\frac{\partial \theta}{\partial z}, \tag{10.1}$$

g is the acceleration due to gravity, and θ is the atmospheric potential temperature (K). This is the frequency at which a vertically displaced air parcel oscillates within a statically stable environment ($N^2 > 0$). Air easily flows over any obstacles to the flow for unstable ($N^2 < 0$) or neutral ($N^2 = 0$) stratification. This is not the case for moderately stable stratification when buoyancy forces are important to the flow over the obstacles and internal gravity waves can be produced (Carruthers and Hunt 1990). As the stratification increases even further, the buoyancy forces are strong enough that vertical motion is suppressed below a certain height and the air flows around the obstacles (Fig. 10.2). Although the height and length of the hill influence the exact response (Carruthers and Hunt 1990), the atmospheric stratification plays the dominant role.

One way to determine whether or not the air flows over or around an obstacle of height h is to examine the inverse Froude number (Fr). This number is defined as

$$Fr = \frac{Nh}{U}, \tag{10.2}$$

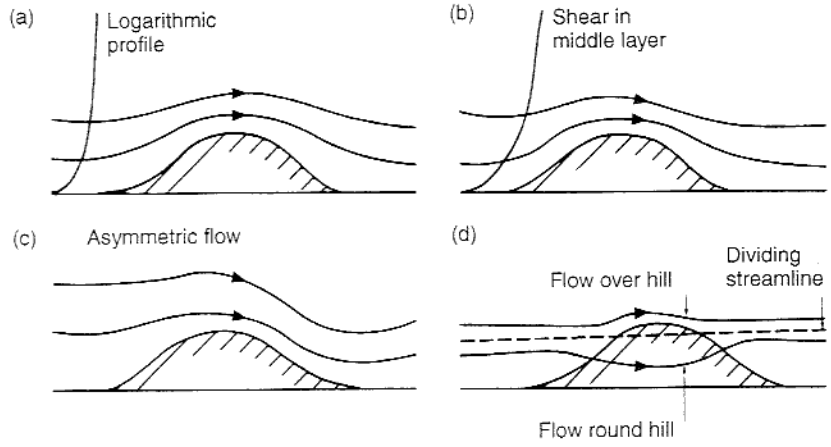

Figure 10.2. Atmospheric flow patterns over a three-dimensional hill for: (a) neutral stratification, (b) weak stratification, (c) moderate stratification, and (d) strong stratification. From Carruthers and Hunt (1990).

where U is the wind speed of the incident flow (Gill 1982). When $Fr \gg 1$ the air flows around the obstacle since the stratification is strong. In contrast, when $Fr \ll 1$ the air flows over the obstacle. For values of $Fr \sim 1$ the air generally flows both around and over the obstacle. As seen in (10.2), for a fixed stratification (N = constant) the value of Fr decreases directly in proportion to increases in the incident wind speed. Thus, both stratification and the incident wind speed are important to determining the influence of the obstacle on the atmospheric flow. The height h of the obstacle also plays a role, as larger heights increase the value of Fr, thereby increasing the likelihood that the flow goes around the obstacle. The amount of drag produced by the obstacle on the atmosphere changes if the flow goes over the obstacle, goes around the obstacle, or if the obstacle generates internal gravity waves, or some combination of these flow responses (Fig. 10.3).

Another important parameter to consider when examining the atmospheric response to obstacles is the Richardson number (Ri), the dimensionless ratio of the buoyant suppression of turbulence to the generation of turbulence by vertical wind shear. It is defined as

$$Ri = \frac{(g/\theta)\,\partial\theta/\partial z}{(\partial U/\partial z)^2} = \frac{N^2}{(\partial U/\partial z)^2}, \tag{10.3}$$

where $U(z)$ is the mean horizontal wind speed. When the Richardson number falls below 0.25, the commonly accepted value of the critical Richardson number, the air becomes unstable and turbulence is generated.

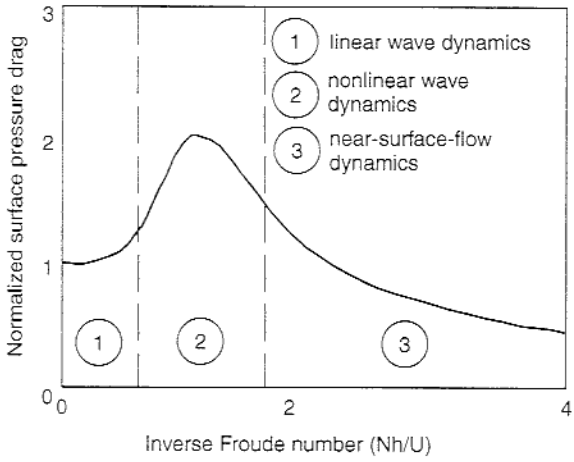

Figure 10.3. Schematic of the normalized surface pressure drag as a function of Fr for constant values of N and U that outlines the three flow regimes identified from the numerical simulations. The pressure drag is normalized by the value expected by linear theory due to freely propagating gravity waves. From Scinocca and McFarlane (2000).

The response of a stably stratified atmosphere to mountains can be investigated analytically following Durran (1986, 1990). For stationary, two-dimensional airflow over small-amplitude mountains the inviscid Boussinesq equations contain the essential physics governing the flow. If these equations are linearized about a horizontally uniform basic state with a mean wind $U(z)$, the result is

$$U\frac{\partial u}{\partial x} + w\frac{\partial U}{\partial z} + c_p\theta_0\frac{\partial \pi}{\partial x} = 0, \tag{10.4}$$

$$U\frac{\partial w}{\partial x} + c_p\theta_0\frac{\partial \pi}{\partial z} = b, \tag{10.5}$$

$$U\frac{\partial b}{\partial x} + N^2 w = 0, \tag{10.6}$$

$$\frac{\partial u}{\partial x} + \frac{\partial w}{\partial z} = 0, \tag{10.7}$$

where $b = g\theta/\theta_0$ and π is the Exner function, which is equal to $(p/p_0)^{R/c_p}$. These equations can be combined to form a single equation in the velocity component w, such that

$$\frac{\partial^2 w}{\partial x^2} + \frac{\partial^2 w}{\partial z^2} + l^2 w = 0, \tag{10.8}$$

in which

$$l^2 = \frac{N^2}{U^2} - \frac{1}{U}\frac{d^2U}{dz^2} \tag{10.9}$$

is the Scorer parameter.

If the terrain height $h(x)$ is assumed to be a series of infinite periodic ridges, an assumption which still retains most of the fundamental properties of small-amplitude mountain waves, then we have

$$h(x) = h_0 \cos(kx), \tag{10.10}$$

where h_0 is the terrain height amplitude and the wavenumber k defines the separation distance of the mountain ridges. It is further assumed that the values of N and U are constant with height and time. Since the terrain surface is fixed and impenetrable, the velocity normal to the topography must vanish. This lower boundary condition requires that

$$w(x, z=0) = (U+u)\frac{\partial h}{\partial x} \approx U\frac{\partial h}{\partial x} = -Uh_0 k \sin(kx). \tag{10.11}$$

Thus, solutions to (10.8) may be written in the form

$$w(x,z) = \hat{w}_1(z)\cos(kx) + \hat{w}_2(z)\sin(kx). \tag{10.12}$$

When this solution is substituted into (10.8), then an equation governing the vertical structure of the perturbation vertical velocity is found, such that both $\hat{w}_1$ and $\hat{w}_2$ satisfy

$$\frac{\partial^2 \hat{w}_i}{\partial z^2} + (l^2 - k^2)\hat{w}_i = 0, \qquad i = 1, 2. \tag{10.13}$$

Since both N and U are assumed to be constant, $l^2 - k^2 = m^2$ is also a constant and the solutions to (10.13) are

$$\hat{w}_i(z) = \begin{cases} A_i e^{\mu z} + B_i e^{-\mu z} & k > l \\ C_i \cos(mz) + D_i \sin(mz) & k < l, \end{cases} \tag{10.14}$$

where $\mu^2 = -m^2$ (Durran 1986). The coefficients A_i, B_i, C_i, and D_i are determined by the boundary conditions at the surface and as z approaches infinity. Since the wave amplitude cannot grow exponentially without bound, it is required that $A_i = 0$. The lower boundary condition (10.11) then defines $B_1 = 0$ and $B_2 = -Uh_0 k$, yielding stationary waves that decrease exponentially with height for $k > l$. For the other case when $k < l$, then trigonometric identities can be used to rewrite the solution for w as

$$w(x,z) = E_1 \sin(kx+mz) + E_2 \sin(kx-mz) + E_3 \cos(kx+mz) + E_4 \cos(kx-mz), \tag{10.15}$$

where $m>0$ and $k>0$. The lower boundary condition leads to $E_1+E_2=-Uh_0k$ and $E_3+E_4=0$.

As discussed by Durran (1986), the terms in (10.15) with $(kx+mz)$ correspond to waves in which the lines of constant phase tilt upstream ($kx+mz=$constant). These waves transport energy upward and momentum downward, which is the desired behavior since the mountain acts as an energy source and the waves should thus transport energy away from the mountain. Note that in this case the horizontal wavenumber k is generally much smaller than the vertical wavenumber m, yielding $m=N/U$ from (10.9). In contrast, the terms with $(kx-mz)$ transport energy downward and towards the mountain – a situation that makes no physical sense. Thus, the upper boundary condition requires that $E_1=-Uh_0k$, and that $E_2=E_3=E_4=0$. Durran (1986, 1990) provides further explanation for this choice of upper boundary condition and why it is the correct one.

Finally, the perturbation vertical velocity field for waves forced by a sinusoidal terrain field defined by (10.10) is given as

$$w(x,z) = \begin{cases} -Uh_0 k e^{-\mu z} \sin(kx) & k>l \\ -Uh_0 k \sin(kx+mz) & k<l. \end{cases} \tag{10.16}$$

These two wave structures are depicted in Fig. 10.4, where the waves with $k>l$ are evanescent waves that decay exponentially with height and the waves with $k<l$ are waves that propagate vertically without loss of amplitude. If ϕ is defined as the angle between the vertical and the slanting parcel trajectories for the vertically propagating waves, then Durran (1986) shows that this angle can be determined from

$$\cos(\phi) = \frac{Uk}{N}, \tag{10.17}$$

as long as $Uk<N$. For $Uk>N$ the waves decay since there is no way for buoyancy forces to support the oscillation.

For more realistic terrain shapes, the terrain profiles are constructed from periodic functions using Fourier transforms (see Durran 1990). Results show that the perturbation vertical velocity over an isolated bell-shaped ridge behaves very similarly to the vertical velocity over the infinite series of sinusoidal ridges. If the mountain quarter width is specified by L, then for a narrow mountain with $N \ll U/L$ the mountain primarily forces evanescent waves. In contrast, for a wide mountain with $N \gg U/L$ the mountain primarily forces waves that propagate vertically and their lines of constant phase tilt upstream.

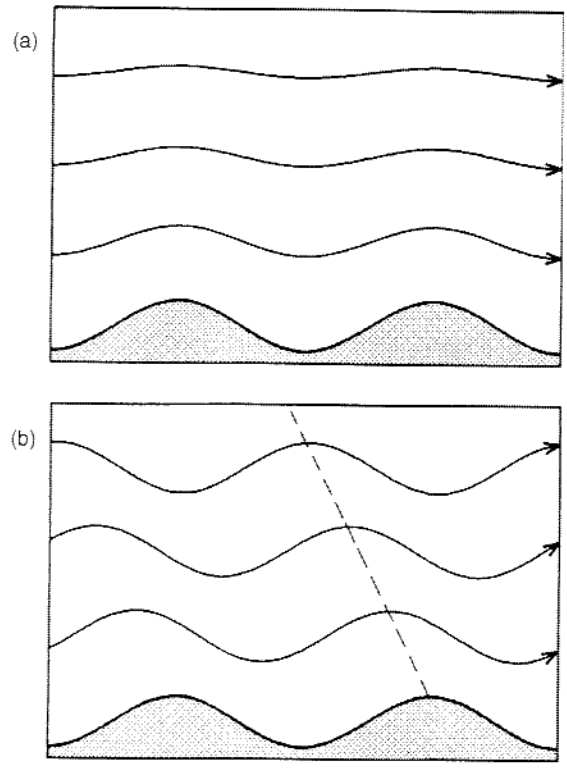

Figure 10.4. Two-dimensional streamlines over an infinite series of sinusoidal ridges for: (a) evanescent waves and (b) vertically propagating gravity waves. The dashed line in (b) indicates the vertical upstream tilt of the lines of constant phase. The airflow is from left to right. From Durran (1990).

When U and N vary in the vertical direction, another type of mountain wave – the trapped lee wave – can occur (Fig. 10.5). In this case the wave activity is confined to the lower troposphere on the lee side of the mountain (Scorer 1949; Durran 1986). If one assumes two vertical atmospheric layers with different values of N in each layer, a necessary condition for the existence of trapped waves can be determined that depends upon the value of the Scorer parameter in each layer and the depth of the lower layer (Scorer 1949). These trapped waves propagate vertically in the lower layer and then decay exponentially with height in the upper layer. The wave energy is repeatedly reflected from the flat ground downstream of the mountain and from the upper atmospheric layer, producing waves with no vertical tilt (Durran 1990). Thus, trapped lee waves are referred to as resonant waves when these conditions are met.

Internal gravity waves are important to the large-scale atmosphere because they can produce drag. If the variables in the horizontal equation of motion

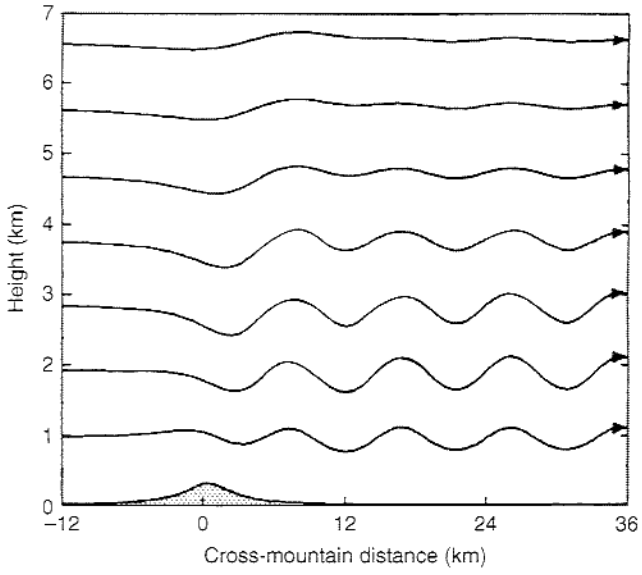

Figure 10.5. Two-dimensional streamlines in steady airflow over a single mountain ridge when the Scorer parameter varies in the vertical allowing trapped lee waves. The airflow is from left to right. From Durran (1990).

written in z coordinates are separated into mean (bar) and perturbation (prime) quantities, then it can be shown that

$$\bar{\rho}\frac{d\bar{V}_H}{dt} + \nabla_H \bar{p} + fk \times \bar{V}_H = -\frac{\partial}{\partial z}(\overline{\rho w' V_H'}) + \cdots, \tag{10.18}$$

where the first term on the right-hand side is the vertical eddy stress convergence term due to gravity waves (Lilly 1972). In a stably stratified atmosphere, gravity waves are able to transport momentum substantial distances between their sources and sinks without affecting the intervening vertical layers (Bretherton 1969). In essence, $\overline{\rho w' V_H'}$ is non-zero when small-amplitude waves are present, but its vertical derivative is zero (Eliassen and Palm 1961). This also implies that the momentum flux for vertically propagating waves at any vertical level is equal to their momentum flux, or stress, at the ground surface in the absence of dissipation (Eliassen and Palm 1961). Drag is produced when the momentum flux changes with height, which occurs during wave breaking and for trapped waves (Durran 1990).

Wave breaking occurs when the gravity waves grow to large amplitude, in part due to the decrease of density with height, and overturn. This occurs because as the amplitude of the waves increases, the influence of the wave circulations on the local environment may lead to the local Richardson number (Ri) dropping below its critical value of 0.25 (Lindzen 1981). Turbulence is then generated,

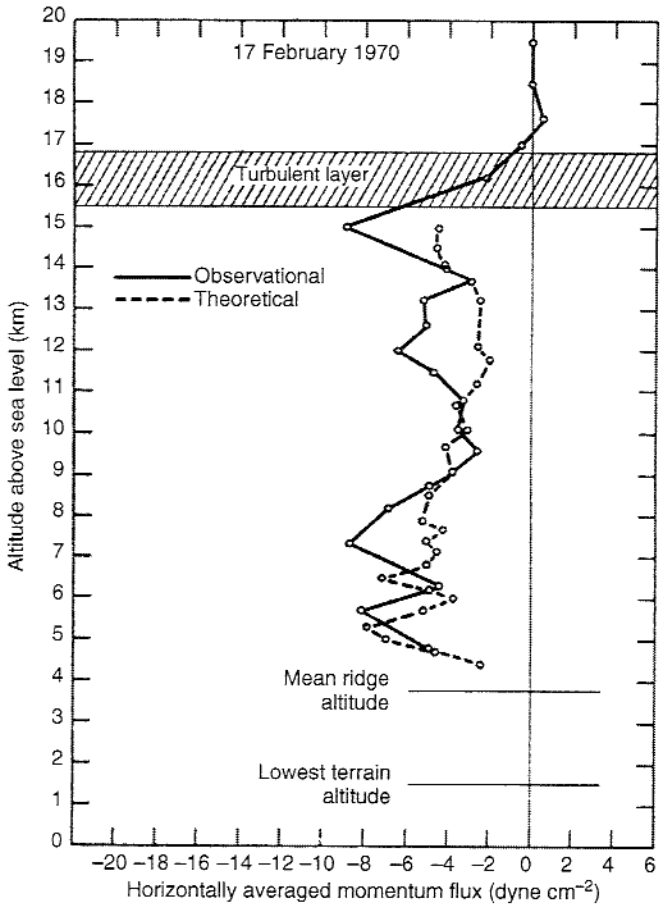

Figure 10.6. Mean observed profile of momentum flux obtained by averaging values obtained from three different analysis methods (solid black line) and from theory (dashed line). Note how the momentum flux is approximately constant with height below the turbulent layer, and then decreases to zero within the turbulent layer. From Lilly and Kennedy (1973).

producing an exchange of momentum between the waves and the environment and hence drag. Analyses of aircraft observations of mountain wave momentum flux indicate that the momentum flux is fairly constant below the turbulent layer (Fig. 10.6) in agreement with theory (Lilly and Kennedy 1973).

Trapped lee waves can also produce momentum flux that varies with height, and produce drag as seen in both model simulations (Durran 1990) and observations (Georgelin and Lott 2001). Although the horizontal average of the momentum flux over one phase of a resonant wave is zero, it is the disturbance nearest the mountain that generates the vertically varying non-zero momentum flux (Durran 1990). Although likely not as important as wave breaking, the drag

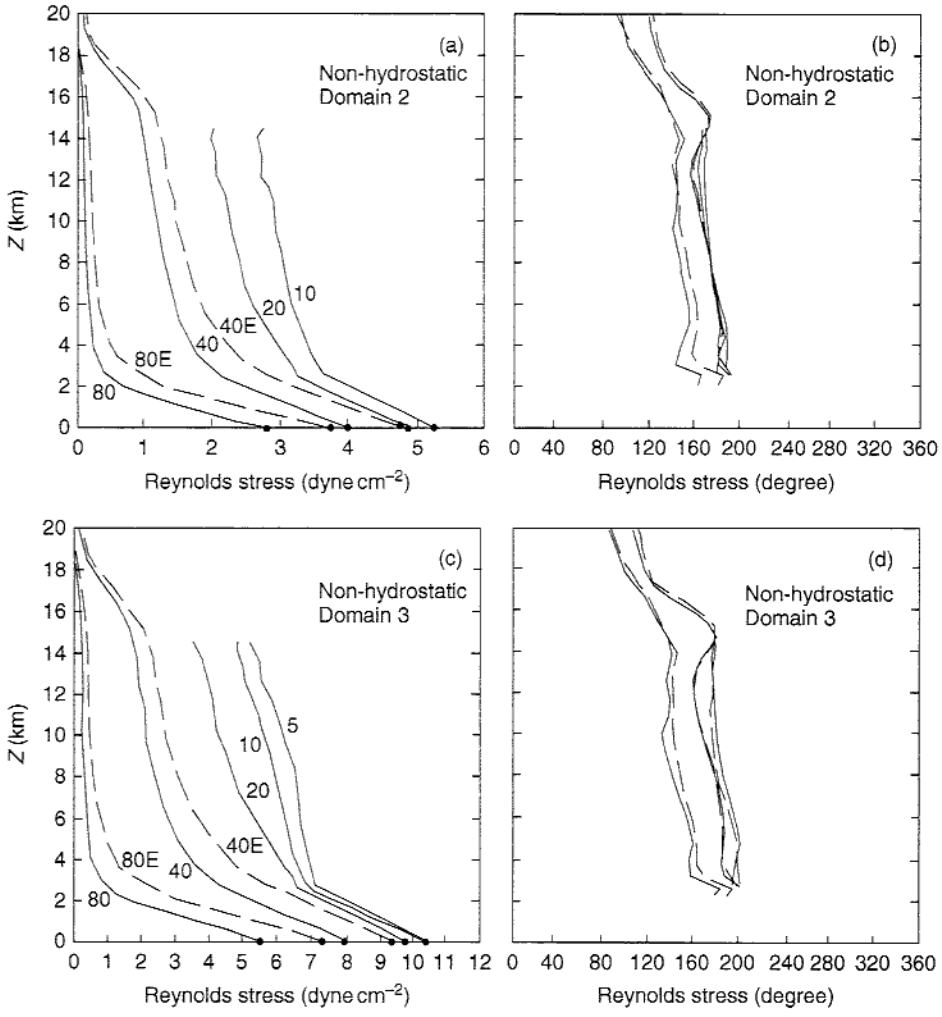

Figure 10.7. Vertical profiles of Reynolds stress for various model grid spacings over the Alps region in northern Italy. Numbers 80, 40, 20, 10, and 5 denote the model grid spacing used, while the letter E refers to a model simulation with envelope orography. The magnitude of the Reynolds stress is on the left, while the direction of the stress is on the right. It is clear that the Reynolds stress at 80 km grid spacing is an order of magnitude smaller above 3 km than the stress determined using 5 km grid spacing, illustrating the need for orographic drag parameterizations. From Clark and Miller (1991).

due to trapped lee waves is a potentially important source of orographic wave drag, especially for models with smaller grid spacing.

The dependence of this vertical momentum flux on model grid spacing is examined by Clark and Miller (1991) for a simulation of flow over the Alps. By

varying the model grid spacing from 80 km to 5 km they show that the vertical momentum flux changes substantially as the grid spacing decreases and conclude that the orographic drag is not fully accounted for in models until the grid spacing falls below 10 km or so (Fig. 10.7). Thus, for many modeling systems it is necessary to parameterize this orographic drag in order to account for its influence on the atmospheric flow.

Orographic drag parameterizations often separate out the effects of low-level flow blocking and gravity wave drag. The total drag due to orography is simply the sum of the drag produced by gravity waves and low-level flow blocking. Whether or not gravity waves or blocking is occurring at a given grid point depends upon the value of the inverse Froude number owing to its ability to describe the response of the atmosphere to an obstacle. An overview of gravity wave drag is conducted first, followed by an overview of the drag from low-level blocking.

10.3 Gravity wave drag parameterizations

There are two parts to most gravity wave drag parameterizations: calculation of the mountain wave stress, or pressure drag, followed by the vertical distribution of the wave stress. For the simplest case of a series of infinite periodic ridges, one can use the perturbation vertical velocity w from (10.16), solve for the perturbation horizontal velocity u using the two-dimensional continuity equation (10.7), and calculate the wave momentum flux or Reynolds stress at the surface from $\tau = \rho\overline{uw}$, yielding

$$\tau_{sfc} = -\frac{1}{2}k\rho UNh_0^2. \tag{10.19}$$

When used in numerical models the stress is often defined similarly as

$$\tau_{sfc} = -B\rho_0 U_0 N_0 h^2, \tag{10.20}$$

where U_0 is the low-level wind speed, N_0 is the low-level Brunt-Väisälä frequency, ρ_0 is the surface density, h^2 is the variance of the subgrid scale orography, and B is a tunable constant that depends upon the characteristics of the orography (Phillips 1984; Palmer *et al.* 1986). For example, Boer *et al.* (1984) define $B \propto 1/d_0$, where d_0 is the typical separation distance between the important topographic features in the grid cell. Kim and Arakawa (1995) show that this type of approach to defining the surface stress due to the mountain waves is fairly common in gravity wave drag parameterizations (e.g., Chouinard *et al.* 1986; McFarlane 1987; Iwasaki *et al.* 1989).

A slightly different formula is developed by Pierrehumbert (1986) in which

$$\tau_{sfc} = -B\frac{\rho_0 U_0^3}{N_0}\left(\frac{Fr^2}{Fr^2+1}\right). \tag{10.21}$$

Assuming that B is constant, then when $Fr \gg 1$ and air flows around the obstacle the surface stress is at its maximum. When $Fr \sim 1$ and air flows both around and over the obstacle, the surface stress is roughly half its potential maximum value. And when $Fr \ll 0$ and air easily flows over the obstacle there is little surface stress. This type of surface stress formulation is used, for example, by Stern *et al.* (1987), Alpert *et al.* (1988), Kim and Arakawa (1995), Gregory *et al.* (1997), and Kim and Doyle (2005).

However, the value of B in (10.20) and (10.21) is not a constant and can vary from gridpoint to gridpoint. The expression for B often is a complicated function of both the subgrid orography and the surface wind direction. For example, Lott and Miller (1997) use estimates of the height variation in the along-ridge and cross-ridge directions to specify the value of B. Estimates of the sharpness, slope, width, and profile of the orography based upon the surface wind direction are used in Kim and Doyle (2005) to calculate B. The formulation in Kim and Arakawa (1995) is based upon results from over 100 two-dimensional mountain wave simulations with various shapes and sizes of mountain. The need for all of these simulations illustrates the sensitivity of the gravity wave drag parameterizations to the subgrid orography and the surface wind direction.

Once the surface stress is determined, the vertical profile of wave stress can be calculated. This is accomplished by estimating the influence of the orographic gravity waves on the local static stability and vertical wind shear and then determining a minimum Richardson number that represents the smallest value the Richardson number can obtain under the influence of the gravity waves. When this minimum Richardson number falls below the critical value for the onset of turbulence, then wave breaking occurs. This minimum Richardson number is defined as

$$Ri_{min} = Ri\frac{1-(N\delta h/U)}{\left[1+Ri^{1/2}(N\delta h/U)\right]^2}. \tag{10.22}$$

where δh is the vertical displacement of an isentropic surface due to the gravity waves, N is the local value of the Brunt-Väisälä frequency, and U is the local wind speed in the direction of the surface wind direction (Palmer *et al.* 1986).

Beginning at the surface, the calculations to determine the gravity wave drag are made by moving upward in the grid cell. The required values of Ri, N, and U are determined directly from the model data for any given vertical level. The value of δh is determined by assuming that the momentum flux at any level

in the atmosphere equals the surface momentum flux unless wave breaking occurs and some of the momentum is transferred to the environment (Eliassen and Palm 1961). Thus, one solves for δh using (10.20) knowing the surface value of the momentum flux (or the momentum flux at the next lowest model level) and replacing the surface values of ρ, N, and U with their values at the given model level. This yields

$$\delta h_i = \left(-\frac{\tau_i}{B\rho_i U_i N_i} \right)^{1/2}, \tag{10.23}$$

where τ_i is the momentum flux reaching to vertical level i and the value of U_i is the component of the wind parallel to the surface wind (Kim and Arakawa 1995). Once the value of δh is determined, the minimum Richardson number is calculated from (10.22). If $Ri_{min} \geq 0.25$, the critical value for the onset of turbulence, then wave breaking does not occur, the vertical wave momentum flux is unchanged, and the next highest vertical level is evaluated. When $Ri_{min} < 0.25$ at a given vertical level in the grid cell, wave breaking occurs and some of the wave momentum flux is transferred to the environment, producing drag.

The most common approach to specifying the amount of momentum flux transferred to the environment is based upon the saturation hypothesis of Lindzen (1981), in which dissipation processes are assumed to limit the wave amplitudes and to produce drag. When wave breaking occurs, one can calculate the value of δh needed to reset the value of Ri_{min} to 0.25 in (10.22) and thus cause the turbulence to cease. The momentum flux that remains after wave breaking is determined using this modified value of δh in (10.20). The difference between the original surface momentum flux and the momentum flux left after wave breaking represents the amount of momentum transferred to the atmosphere at the model level height. Several caveats and practical points regarding these calculations are discussed by Palmer *et al.* (1986).

A comparison of results from a gravity wave drag parameterization that is based upon the saturation hypothesis with results from two-dimensional mountain wave simulations suggests that the magnitude of the parameterized drag is underestimated in low-level downstream regions with wave breaking or lee wave trapping (Kim and Arakawa 1995). Further exploration of this problem by Kim and Arakawa (1995) suggests that the vertical gradient of the Scorer parameter is a more useful approach to estimating the change of wave momentum flux with height at low levels. Thus, the change in wave momentum flux is defined using

$$\frac{\tau_i}{\tau_{i-1}} = \min\left(C_i \frac{l_i^2}{l_{i-1}^2}, 1 \right), \tag{10.24}$$

where $C_i = 1$ (a tunable constant), i defines the vertical model layer and increases upwards, and l is again the Scorer parameter (Kim and Arakawa 1995; Kim and Doyle 2005). Kim and Arakawa (1995) use (10.24) to determine the change in wave momentum flux below 10 km and use the saturation hypothesis (10.22) above 10 km.

The effects of low-level wave breaking within the first vertical wavelength above the surface also can be approximated by examining the results from fully three-dimensional simulations of breaking waves. Results indicate that the surface stress is amplified by up to three times above expectations from linear theory for flow over obstacles, and this stress amplification depends upon the value of *Fr* (see Fig. 10.3). Thus, Scinocca and McFarlane (2000) develop a simple empirical relationship to increase the surface stress for the appropriate range of *Fr* values for which low-level breaking is likely. This stress decreases linearly between the surface and the height of wave breaking. Kim and Doyle (2005) include an enhancement factor in their calculation of low-level drag to account for low-level wave breaking and wave trapping, which is also tied to the value of *Fr*.

Most gravity wave drag parameterizations assume only one vertically propagating gravity wave is generated by the subgrid orographic mountains. When the model winds turn with height and become normal to the surface wind direction (i.e., the two-dimensional wave orientation) a critical level is created and all of the remaining wave momentum is transferred to the atmosphere at this one vertical level. This can result in excessive momentum deposition at these critical levels (Scinocca and McFarlane 2000). To help alleviate this problem, Scinocca and McFarlane (2000) assume that there exist two vertically propagating gravity waves within each grid cell with different orientations, while Gregory *et al.* (1997) assume a finite spectrum of gravity waves. Most models that focus upon the evolution of the atmosphere in the troposphere assume a single gravity wave, whereas models that also need to predict the evolution of the stratosphere tend to allow for a spectrum of waves (Kim *et al.* 2003).

10.4 Low-level blocking drag parameterizations

The blocking of low-level flow due to subgrid-scale mountains also can produce an extra source of drag for the atmosphere. Initial attempts to account for this blocking effect focused upon modifying the model-resolved orography. For example, the original model terrain heights (i.e., the average terrain height within a model grid cell) are increased in proportion to the standard deviation of the subgrid terrain heights when applying envelope orography (Wallace *et al.* 1983). A similar approach is used by Mesinger *et al.* (1988) in a study of lee cyclogenesis in which the model terrain heights are defined by the tallest

peaks and by Tibaldi (1986) in studying the maintenance of quasi-stationary waves. However, while these approaches increase the drag, since the terrain is taller and interacts with a deeper layer of the atmosphere, they also appear to have undesirable consequences. Envelope orography makes the assimilation of low-level observations more difficult, while also leading to excessive precipitation over the enhanced orography (Lott and Miller 1997).

The problems with envelope orography and other modifications to the original average model terrain field led to the development of low-level blocking parameterizations. These approaches use the value of the inverse Froude number to estimate the depth of the flow that is blocked by the subgrid mountains. Scale analysis and results from analytic studies of flow over objects of various shapes allow for an estimation of the surface form drag due to subgrid orographic features. A typical form of the surface stress due to low-level blocking is

$$\tau_{sfc} = -\frac{\Lambda}{2L^2}\rho_0 C h_b l_b U_0 |U_0|. \tag{10.25}$$

where L^2 is the area of the grid cell, Λ is an estimate of the number of ellipses needed to represent the unresolved topographic features, C is a bulk drag coefficient, h_b is the height of the blocked layer, and l_b is the width of the blocked layer (Scinocca and McFarlane 2000). An alternative formulation to (10.25) is found in Kim and Doyle (2005) that includes a unique set of parameters that take into consideration the details of the orographic configurations. The height of the blocked layer is related to the inverse Froude number, such that

$$h_b = \frac{U_0}{N_0}[Fr - Fr_c]. \tag{10.26}$$

where Fr_c is the critical inverse Froude number that specifies when low-level wave breaking occurs and has a value of $\sim$1 (Scinocca and McFarlane 2000). Over the depth of the blocked flow region the stress is typically held constant or decreased linearly with height (Lott and Miller 1997; Scinocca and McFarlane 2000).

10.5 Discussion

Most orographic drag parameterizations used within operational forecast models today are based upon a combination of low-level blocking and gravity wave drag diagnostic calculations. We have seen that these calculations depend upon the values of N, U, and Fr, and the variation of the orography within the model grid cell. The amount of drag imparted to the atmosphere also depends upon the assumptions used for determining where and when wave breaking occurs. While most of the early orographic drag parameterizations

were evaluated only by their ability to improve the model forecasts, most studies today also try to evaluate the parameterizations off-line in comparisons with observations from a handful of field campaigns and wave-resolving model simulations (Kim *et al.* 2003). For example, the orographic drag parameterization of Kim and Doyle (2005) is compared with simulations that explicitly resolve the momentum flux over complex orography. Results suggest good agreement between the parameterization and the explicit momentum flux calculations (Fig. 10.8). However, the objective evaluation of orographic drag parameterizations remains difficult and many of the parameters used within these schemes are not constrained and so must be selected carefully.

The need for gravity wave drag also is not limited to flow over mountain ranges. Deep convection also produces gravity waves that propagate vertically and may need to be parameterized (Lindzen 1984; Kershaw 1995; Gregory *et al.* 1997; Bosseut *et al.* 1998; Chun and Baik 1998, 2002). It appears that organized convective regions, such as mesoscale convective systems, may be important generators of gravity waves that influence atmospheric circulations in the Tropics (Kim *et al.* 2003). In particular, Alexander and Holton (1997) hypothesize that convectively generated gravity waves are a possible mechanism for the quasi-biennial oscillation. Unfortunately, developing parameterizations for convectively generated gravity waves is even more challenging than for the orographically generated gravity waves, in part because the generated waves are largely non-stationary and there are a number of mechanisms that can account for the wave generation.

One of the challenges to orographic drag parameterizations is the ever changing grid spacing of the models. For large horizontal grid spacings the gravity waves forced by convection or terrain likely remain contained within the model grid cell to a first approximation. However, as the grid spacing is reduced it is possible and perhaps even likely that the gravity waves actually propagate out of the model vertical grid column to influence neighboring grid points. Methods to approximate this wave propagation into neighboring grid cells have been developed, but are presently too computationally expensive for widespread use (Kim and Doyle 2005). The vertical grid spacing is also likely to be an important consideration as it influences the predicted values of U and N.

The length of the model simulation also is an important consideration when deciding if an orographic drag parameterization is needed. Certainly for model forecasts beyond a few days the potential influences of orographic drag are large enough to warrant inclusion of the parameterization. However, the strong mixing and drag produced by wave breaking associated with downslope wind storms can be substantial even for shorter time periods. Thus, these types of parameterizations may need to be included even for

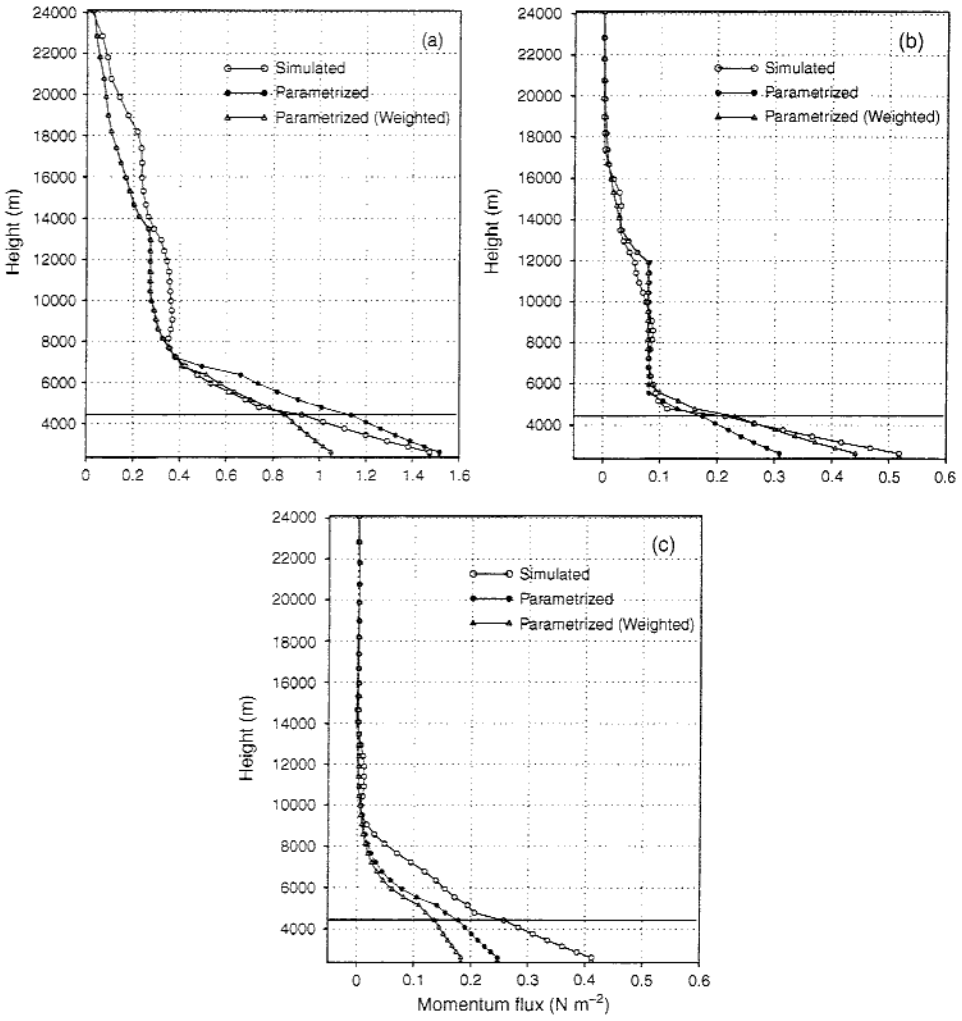

Figure 10.8. Momentum flux from an orographic drag parameterization compared with the flux calculated from an explicit 2 km grid spacing simulation of the gravity wave event produced by flow over mountains. The sign of the momentum flux is reversed. Results from three different cases are shown. In (a) the momentum flux does not reach 0 below 24 km. In (b) the momentum flux goes to zero between 8 and 18 km, whereas in (c) the momentum flux goes to zero below 14 km. From Kim and Doyle (2005).

short-range forecasts. The point at which the horizontal grid spacing begins to fully resolve the gravity waves, such that no orographic drag parameterization is needed, also remains an open question (see Kim *et al.* 2003). The effects of moisture on the development of trapped mountain waves also may be important, as the wave response can be amplified or damped due to the presence of moisture (Durran and Klemp 1982; Kim and Doyle 2005).

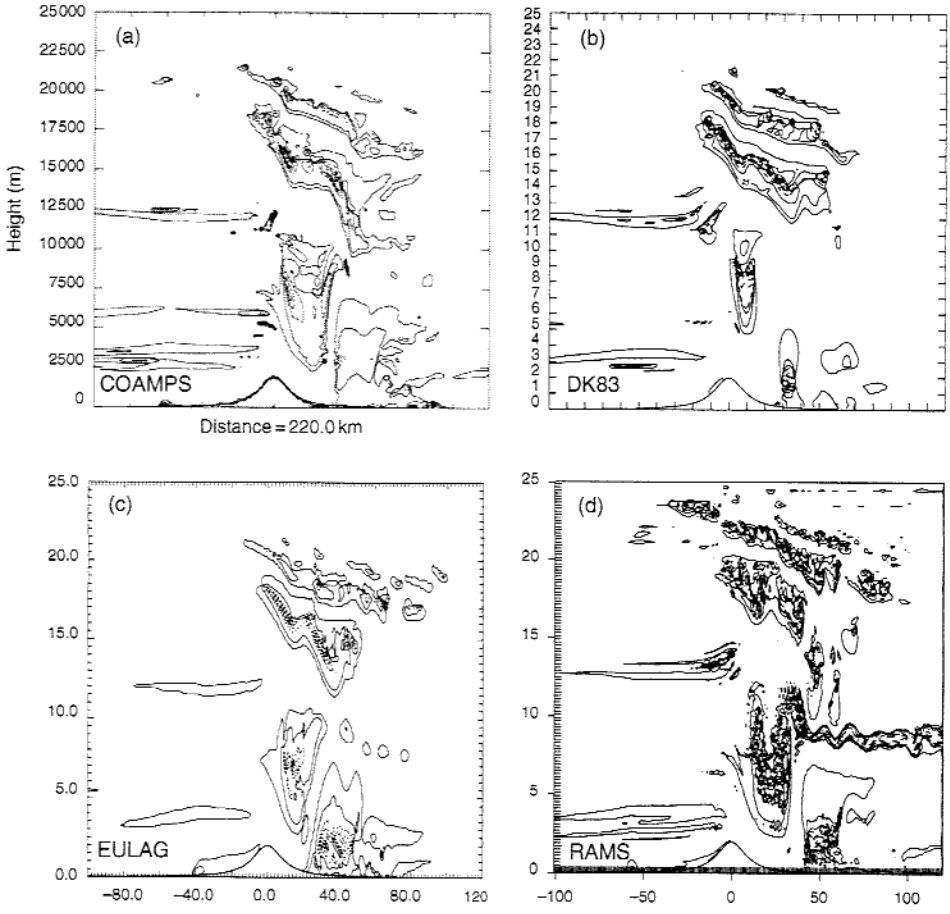

Figure 10.9. Isolines of sign(Ri) $|Ri|^{1/2}$ at the 3 h time from idealized simulations of the 11 January 1972 Boulder, Colorado, downslope windstorm using 4 different non-hydrostatic models. All simulations are two-dimensional and use an idealized mountain profile. While the general regions of wave breaking are very similar, the details are very different. From Doyle *et al.* (2000).

Explicit two-dimensional simulations of gravity wave breaking over an analytic orographic profile from 11 different numerical models show many similarities (Doyle *et al.* 2000). All the runs produce wave breaking in approximately the same location in the stratosphere and produce downslope winds in the lee of the mountain. However, there also are notable differences in the details of the strength of the downslope winds, the depth of the wave breaking region, and the detailed structures within the breaking region (Fig. 10.9). So while these results are encouraging in that all the models produce wave breaking, they also raise some concerns about the ability of explicit gravity wave simulations to produce accurate reproductions of all aspects of the wave breaking. Since wave breaking is a very non-linear process (Peltier and Clark

1979) this is probably not a surprising result. The difficulty becomes trying to parameterize a highly non-linear process based upon the resolved model variables. This process is very challenging, yet the developers of orographic drag parameterizations strive to provide realistic estimates of drag for use in a variety of numerical weather prediction models.

10.6 Questions

1. Using the sounding data listed below, plot the sounding on a thermodynamic diagram, and calculate the values of N using (10.1) for each height level.
2. Assume that a mountain exists near this sounding location with a ridge orientation of 180°. Vary the mountain height between 100 and 500 m in 50 m increments, and calculate the inverse Froude number using (10.2). What type of atmospheric response would be expected from this obstacle to the flow?
3. Given a surface stress of $-1.0\,\mathrm{kg\,m^{-1}\,s^{-2}}$ and $B=0.2$, calculate δh and Ri_{min} for each height level using (10.22) and (10.23). Explain the mechanics of this calculation and any assumptions made. Would wave breaking occur?
4. Increase the values of N in the column by 10%. How does this change the expectations for wave breaking?
5. Increase the values of wind speed normal to the ridge orientation by 10%. How does this change the expectations for wave breaking?
6. Decrease the value of B from 0.2 to 0.1. Describe the changes to the values of Ri_{min}.
7. Using the results of Questions 3–6, discuss the sensitivities of the parameterization scheme to the model forecasts of the environment that the schemes use to predict orographically produced gravity waves.

Sounding data for use in Questions 1–7.

P (hPa)	H (m)	T (°C)	TD (°C)	U ($\mathrm{m\,s^{-1}}$)
861	1 475	−2.90	−6.40	2.00
850	1 573	0.00	−8.00	8.00
813	1 930	0.20	−13.80	6.00
762	2 438	−1.80	−10.73	0.70
726	2 831	−1.90	−8.90	3.00
700	3 120	−4.30	−11.30	7.00
653	3 658	−6.20	−15.94	8.00
604	4 267	−9.90	−21.35	14.00
500	5 710	−19.10	−39.10	16.00
400	7 320	−32.30	−48.30	20.00
300	9 300	−45.30	−55.30	25.00
250	10 500	−52.50	−61.50	41.00
200	11 920	−55.30	−71.30	25.00
150	13 750	−56.70	−80.70	20.00
100	16 270	−64.90	−87.90	15.00